

Scanning X-ray interferometry and the silicon lattice parameter: towards 10^{-9} relative uncertainty?

A. Bergamin¹, G. Cavagnero¹, G. Mana^{1,a}, and G. Zosi²

¹ CNR, Istituto di Metrologia “G. Colonnetti”, strada delle Cacce 73, 10135 Torino, Italy

² Università di Torino, Dipartimento di Fisica Generale, via P. Giuria 1, 10125 Torino, Italy

Received 13 August 1998

Abstract. In order to reduce measurement uncertainty of the (220) lattice spacing of silicon to a few parts per 10^9 , a combined X-ray and optical interferometer capable of millimeter scans is being tested. A new series of measurements confirmed the value obtained with our previous set-up, and the bounds of measurement uncertainty were investigated. The article supplements the analysis of the error budget and provides a safer footing for the monocrystalline silicon lattice parameter value.

PACS. 06.20.Jr Determination of fundamental constants – 06.30.Bp Spatial dimensions (e.g., position, lengths, volume, angles, displacements, including nanometer-scale displacements) – 61.10.-i X-ray diffraction and scattering

1 Introduction

The Committee on Data for Science and Technology of the International Council of Scientific Unions is engaged in refining the self-consistent set of values of the basic physical constants recommended for use in science and technology [1]. Among these, the (220) silicon lattice spacing, d_{220} , is very important for the extension of the electromagnetic scale toward the γ -ray region [2] and for the determinations of the Avogadro [3, 4] and fine structure [5] constants.


Having obtained a value with 3×10^{-8} relative uncertainty by operating a combined X-ray and optical interferometer over an 80 μm scan, we decided for two reasons to improve X-ray and laser interferometry. First, in the X-ray crystal-density determination of the Avogadro constant, the uncertainties of the measurements of silicon density and molar mass are being reduced to the extent that the contribution of the d_{220} value to the N_A uncertainty may become no longer negligible. Second, the largest contribution to the uncertainty of the fine structure constant value obtained from the measurement of the de Broglie wavelength of thermal neutrons is due to the d_{220} value.

We thus designed a scanning device capable of millimeter displacements with which we carried out additional measurements; we reconsidered the overall error and investigated some critical aspects of X-ray and laser interferometry. The analysis of the new data led us to conclude that a 10^{-9} measurement uncertainty is not beyond experimental capabilities. This article is an account of the research thus far completed: it gives the results of the in-

vestigations, supplements the analysis of the d_{220} error budget, and describes future plans for the experiment.

2 Experimental set-up

To measure the (220) silicon lattice spacing we use a combined X-ray and laser interferometer situated in a vacuum-tight and temperature-controlled chamber. Figure 1 shows a diagram of the X-ray and optical interferometers. Since detailed descriptions of their operation and of the measurement procedure are reported elsewhere [6–13], we give here only a brief account. The lattice spacing is obtained by counting the number of (220) planes in a crystal portion of known length; for this an X-ray interferometer and a laser interferometer must be so coupled as to have the same baseline, along which a silicon crystal, which is a part of the X-ray interferometer known as the analyser, is moved orthogonally to the (220) planes. The outgoing X-rays are intensity modulated as the analyser moves, and the number of lattice planes passing is indicated by the number of traveling fringes. Therefore, what is measured is the number of traveling X-ray fringes in a given crystal displacement, which is equal to an integer number of optical periods. To avoid counting all the lattice planes, we measure the excess fraction of X-ray fringe at the ends of displacements of increasing length (the progression used was 1, 10, 100, 1000, and 5000 optical periods) and increase the accuracy step by step. There is always a small residual drift between the X-ray and laser interferometers; therefore, values are corrected by averaging the results of a sequence of displacements in opposite directions; each measurement takes about one hour.

^a e-mail: g.manaimgc.to.cnr.it

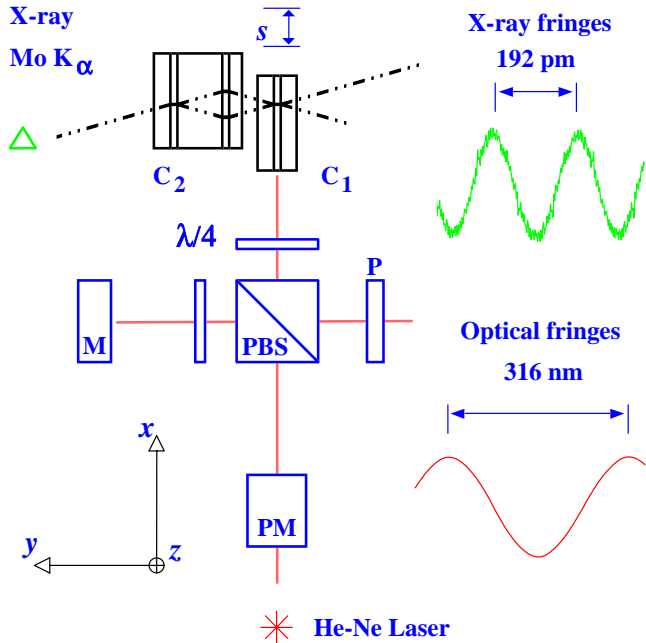


Fig. 1. Diagram of the combined X-ray and optical interferometers. C1 and C2 movable (analyser) and fixed crystals of the X-ray interferometer, M fixed mirror of the laser interferometer, P polariser, PBS polarising beam splitter, PM phase modulator, s analyser displacement.

3 Remeasurement of lattice spacing

For the remeasurements, we used the same X-ray interferometer (labeled MO*4) as described in [6,7], but the experimental apparatus was taken apart and reassembled, the laser source replaced and the guiding device significantly improved. The relatively short scan, 80 μm , was one of the factors limiting the accuracy of the value we reported in [6,7]. The combination of finite-element analysis and active control allowed us to achieve millimeter displacements by constructing an elastic guide capable of scan velocity from 1 pm/s to 0.1 mm/s and of translations up to 2 mm, smooth to within 1 pm, with yawing and pitching to within 1 nrad [14]. An example of the capabilities of the new set-up is given in Figure 2. It shows the histogram of 45 consecutive measurements of the number of X-ray fringes per optical period. In order to achieve maximum resolution, we counted the number of X-ray fringes in 5000 optical periods, about 1.6 mm. The standard deviations of the single measurement results, estimated from the number of photon detected [15] and represented in the figure by the error bars, is close to the width of the histogram. For the value obtained by averaging the results of a typical sequence of measurements, the standard deviation reduces to below 10^{-9} . This is a key result: over one hour time scales, the biggest contribution to data spread is made by the photon count and our set-up is suitable to investigate systematic errors down to a relative magnitude of 10^{-9} . Figure 3 gives a second example. In this group of measurements, the wavelength of the stabilised laser source was intentionally varied from that of the com-

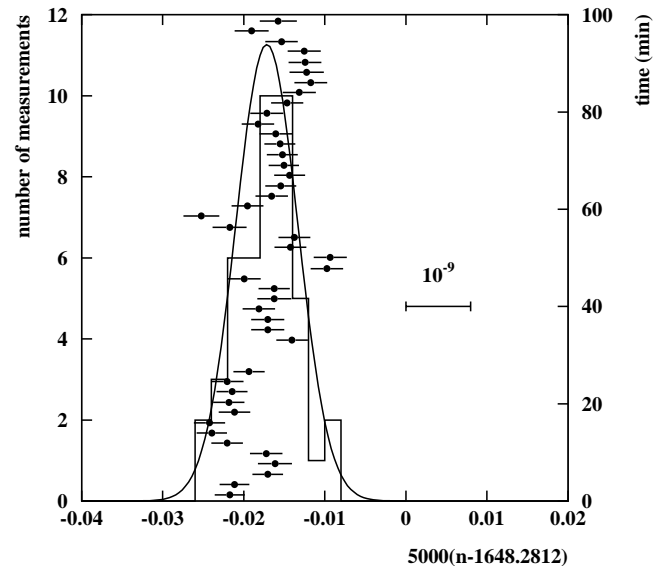


Fig. 2. Histogram of 45 measurement results of n , the number of X-ray fringes (lattice planes) per optical period. Solid line is the best fit of data to a Gauss distribution. All values are reduced to 22.5 $^{\circ}\text{C}$, but are not otherwise corrected.

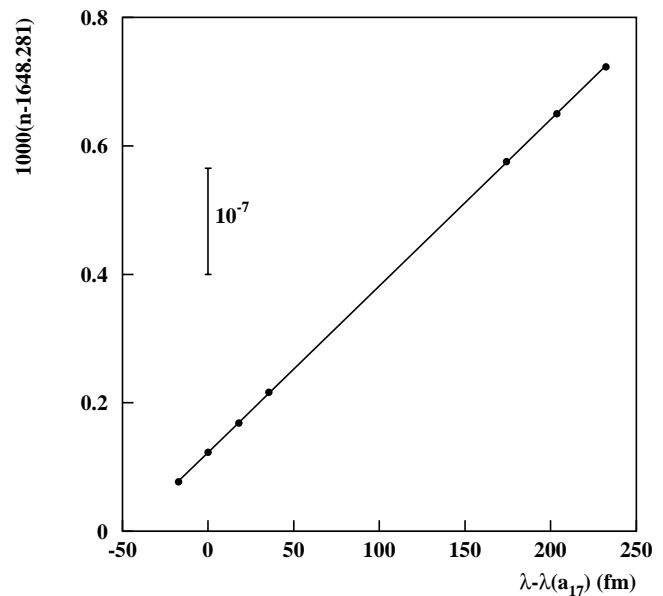


Fig. 3. Number of X-ray fringes per optical period, n , versus wavelength of the stabilised laser radiation. The absorbing molecule is $^{127}\text{I}_2$. Dots relate to components from a_{12} to a_{18} of the transition 11-5, R(127). Solid line is the best fit of data to a straight line.

ponent a_{12} to that of the component a_{18} of the transition 11-5 R(127) of the $^{127}\text{I}_2$ molecule. As shown in the figure, we could detect the linear increase of the X-ray fringes per optical period. Before the lattice spacing value is calculated, the number of X-ray fringes must be corrected for several systematic errors. In order to investigate these errors in-depth, several sets of measurements were done, and are described below. Table 1 summarises the d_{220}

Table 1. Summary of d_{220} values.

date	value ^a (fm)	remarks
1994	192 015.551(5)	references [11,12]
1996 (October)	192 015.552(4)	crystal temperature
1996 (October)	192 015.552(4)	lattice strain
1996 (November)	192 015.547(4)	crystal movement
1996 (December)	192 015.551(4)	diffraction
1997 (January)	192 015.550(4)	residual pressure

^avalues are not corrected for C and O contents.

Table 2. Corrections and uncertainties ($\times 10^8$).

optical wavelength	-0.4 ± 0.2
Fresnel's diffraction	2.0 ± 1.0
laser beam alignment	0.3 ± 0.4
crystal temperature	0.3 ± 0.5
movement direction	0.0 ± 1.3
Abbe's error	0.0 ± 0.5
lattice strain	0.0 ± 0.8
overall (IMGC crystal)	2.2 ± 2.1

values and indicates the investigation that gave the values reported; Table 2 gives corrections and uncertainties of a typical measurement.

4 Investigation of systematic errors

4.1 Residual pressure

When operating in air, the performances of the combined X-ray and optical interferometer are negatively influenced by the fluctuations of the refractive index of air. Measurements were therefore done in vacuo. In order to evaluate precisely the correction for the residual gas in the vacuum chamber pressure was intentionally varied between $5 \mu\text{bar}$ to $25 \mu\text{bar}$. As Figure 4 shows, we were able to detect the variation of the measured value and the final d_{220} value was obtained by extrapolating the data to a perfect vacuum. The asymptotic value for low pressures of the refractivity per mbar at room temperature obtained from data in Figure 4 is $n - 1 = (3.4 \pm 0.4) \times 10^{-7}$ 1/mbar. Since, according to the Lorenz-Lorentz equation, refractivity is, to within a good approximation, proportional to residual-gas density, this value can be compared with the value 2.7×10^{-7} 1/mbar, obtained by dividing refractivity of standard air at room temperature by 1013 mbar [16].

4.2 Crystal temperature

Since lattice spacing is a function of the crystal temperature, its value, to be meaningful, must be referred to a

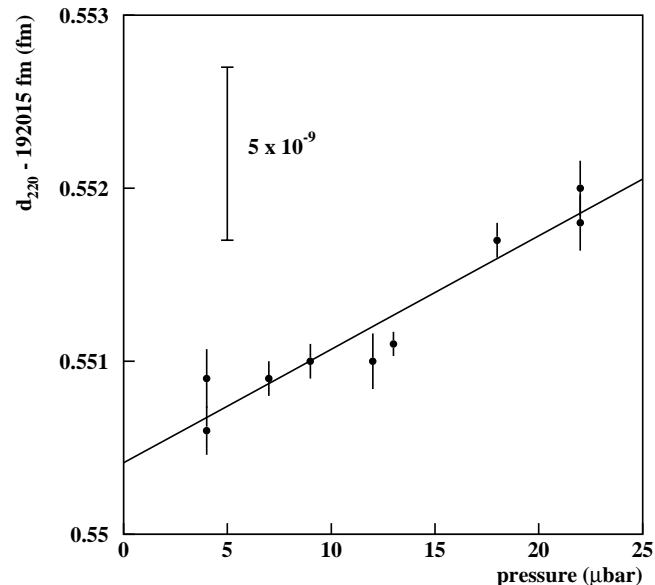


Fig. 4. Effect of residual gas in the vacuum chamber on the result of the d_{220} measurement. Solid line is the best fit of data to a straight line.

reference temperature, established in our normal practice at $22.5 \text{ }^\circ\text{C}$, by applying a correction for thermal strain. However, the thermal expansion values reported in the literature vary by more than the targeted d_{220} uncertainty. Furthermore, most of the published data concerns smooth approximating functions covering a temperature range wider than necessary. Thermal expansion at a given temperature can only be determined by measuring crystal expansion over a small temperature range.

In the measurements, temperature was varied between $21.0 \text{ }^\circ\text{C}$ and $23.5 \text{ }^\circ\text{C}$ and a polynomial approximation for the thermal expansion coefficient was accurately determined. A detailed description of these measurements and the results are reported in [17]. As shown in Figure 5, we observed the thermal strain of the silicon lattice and the final d_{220} value was obtained by interpolation. Hence, temperature correction was made according to first order polynomial approximation

$$\alpha(T) = \alpha_0 + \beta\Delta T \quad (1)$$

where ΔT is the temperature deviation from $22.5 \text{ }^\circ\text{C}$, and

$$\alpha_0 = (2.581 \pm 0.002) \times 10^{-6} \text{ 1/K} \quad (2a)$$

and

$$\beta = (0.016 \pm 0.004) \times 10^{-6} \text{ 1/K}^2 \quad (2b)$$

have been obtained from data in Figure 5.

4.3 Diffraction in laser interferometry

We identified diffraction as an important source of errors, and measurement results needed to be corrected by $\theta^2/4$,

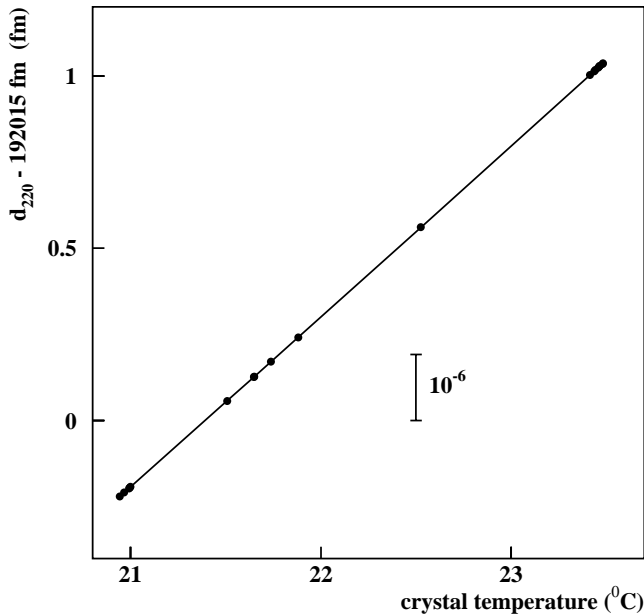


Fig. 5. Thermal expansion of (220) lattice planes. Solid line is the best fit of data to a parabola.

where θ is the divergence of the laser beam. We studied diffraction by using the Gaussian approximation [18] of the laser beam, and then we extended the analysis to beam shear [19] and astigmatism [20]. However, millimeter scans, permitting an increase of one order of magnitude in resolution, put the matter in a different light. The laser beam is delivered by means of a single-mode polarisation-preserving optical fibre whose output is collimated by means of a high-numerical-aperture lens. A way to minimise the correction for diffraction is with the collimating lens, but the lens introduces aberrations, chiefly spherical aberration and beam truncation. Although we are looking at remedies, the perfection represented as a Gaussian beam can never be actually attained. The potential 10^{-9} accuracy raises thus questions about correction calculation and about the assessment of how close the beam is to the perfection represented, conceptually, as a Gauss function.

The operation of the laser interferometer was therefore studied using Fourier optics [21]. The main results were, firstly, that the correction for diffraction is proportional to the width of the angular spectrum of the field distribution over the interferometer aperture and, secondly, that, provided it is expressed in terms of the far-field divergence, the correction is given by the same formula as for a Gauss distribution, no matter what the actual field distribution may be. A third key result is that minimum correction is made for a Gauss distribution.

In order to investigate this error in depth we enhanced diffraction by varying the aperture of the laser interferometer from 1 mm to 6 mm with an iris diaphragm. Results are shown in Figure 6. The correction expected for a truncated Gauss distribution with circular symmetry was calculated, and the waist size of the incoming beam adjusted until observations were reproduced. The best fit of

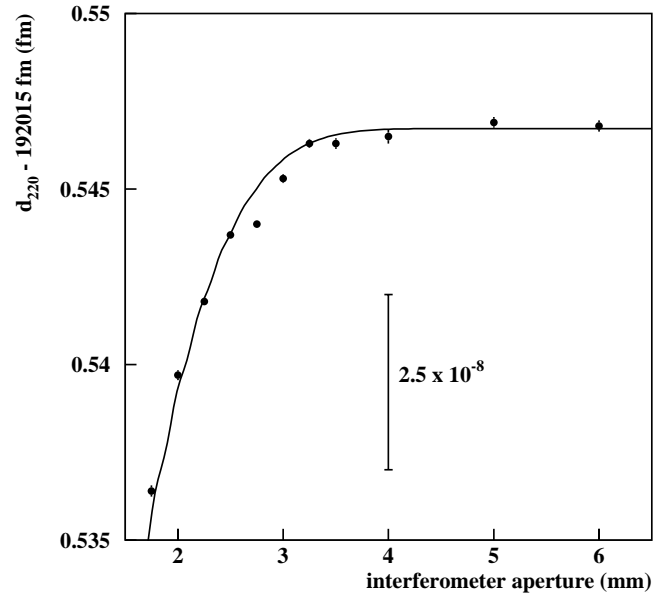


Fig. 6. Effect of the aperture of the laser interferometer on the result of the d_{220} measurement. Solid line is the best fit of data to the predicted function.

data to the predicted function was when the waist size was 2 mm ($1/e^2$ diameter). Although, within the limits of this qualitative investigations, this waist size agrees with the value obtained by measuring the far-field divergence, we cautiously rounded diffraction correction to 2×10^{-8} .

4.4 Lattice strains

The targeted accuracy also raises questions about the value to be attributed to an ideal undistorted crystal, of which MO*4 is an approximate realisation. Long range strains were investigated by mapping the lattice spacing along the scan direction. X-rays were shifted in 0.2 mm steps and lattice spacing was measured in 45 adjacent crystal slabs. Results are in Figure 7, and show that, when the X-rays location is changed, measurement reproducibility is lost. However, lattice spacing does not uniquely determine the period of X-ray fringes unless the movable crystal is free from thickness variations [22–25] and, owing to limits of manufacturing accuracy, the thickness of the MO*4 crystal changes from one point to the next. Although, in principle, aberrations can be separated from lattice strains by their different effects on fringes of transmitted and reflected beams, our present set-up did not prove capable of such a separation and, consequently, there is no single interpretation of data in Figure 7. The final d_{220} value was measured in that part of the crystal which is at 6 mm from the front, and where the d_{220} value is, to within a good approximation, equal to the average.

4.5 Crystal movement

In our experiment, the path of the crystal is an arc lying in the vertical plane, and the local direction of movement,

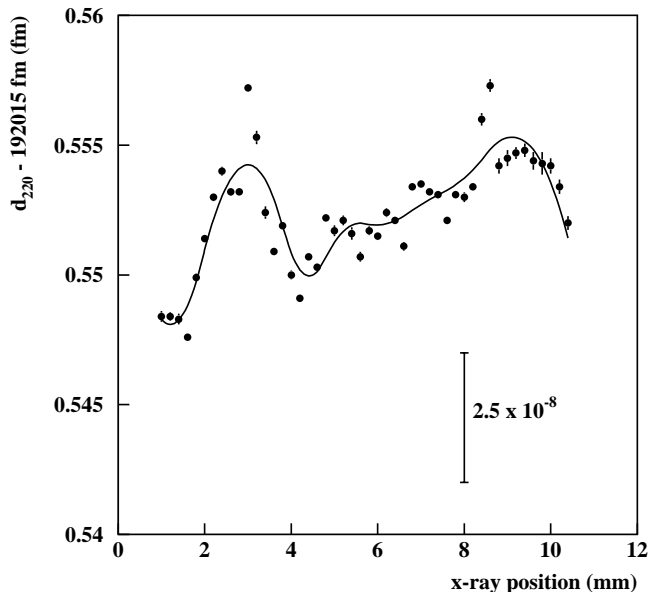


Fig. 7. Map of d_{220} along the scan direction. The solid line is a smooth interpolation between data.

that is the tangent to the path, depends linearly on the position of the crystal [14]. The non-rectilinear path combines with the angle α between the lattice planes and front face of the analyser (the moving mirror of the laser interferometer) and changes the paths which are measured by X-rays and laser interferometer. Let us consider a plane path having a constant curvature R and let us introduce a coordinate s normal to the front face of the analyser. With the simplifying assumption that the laser beam is normal to the front face, s is the quantity actually measured by the laser interferometer. Thus, since the analyser position is

$$\mathbf{u}(s) = s\mathbf{e}_x - \frac{s^2}{2R}\mathbf{e}_z, \quad (3)$$

where \mathbf{e}_x is orthogonal to the front face and \mathbf{e}_z is vertical, the phase of traveling X-ray fringes versus the result of the position measurement is

$$\Phi(s) = \mathbf{h} \cdot \mathbf{u}(s) = h \left[s - \frac{\alpha_z s^2}{2R} \right] \quad (4)$$

where \mathbf{h} , with $h = 2\pi/d_{220}$, is the reciprocal vector and $\alpha_z = \mathbf{h} \cdot \mathbf{e}_z/h$ is the “vertical” component of α . Equation (4) indicates that, when the path is not rectilinear, the number of traveling X-ray fringes no longer increases linearly with the result of the position measurement. Rather, it is a copy of the path, a consequence of having measured displacement along the normal to the front face rather than to the lattice planes. This copying makes the d_{220} value, the derivative of the fringe phase, linearly dependent on the result of the analyser-position measurement. We verified these predictions by using an X-ray interferometer (labeled WASO 4.2A) loaned to us by the Physikalisch-Technische Bundesanstalt (PTB) in which, in spite of the smaller overall angle, α_z is relatively large. Results are shown in Figures 8 and 9. The

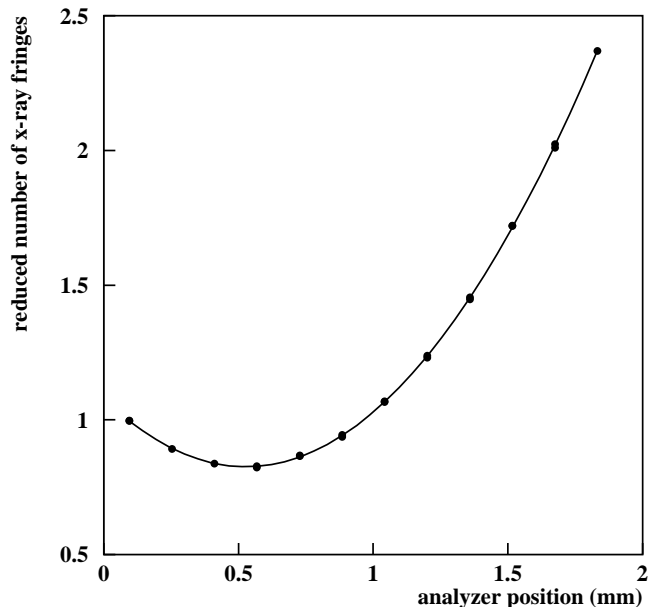


Fig. 8. Phase of travelling X-ray fringes *vs.* the result of the analyser-position measurement. The solid line is the best fit of data to a parabola.

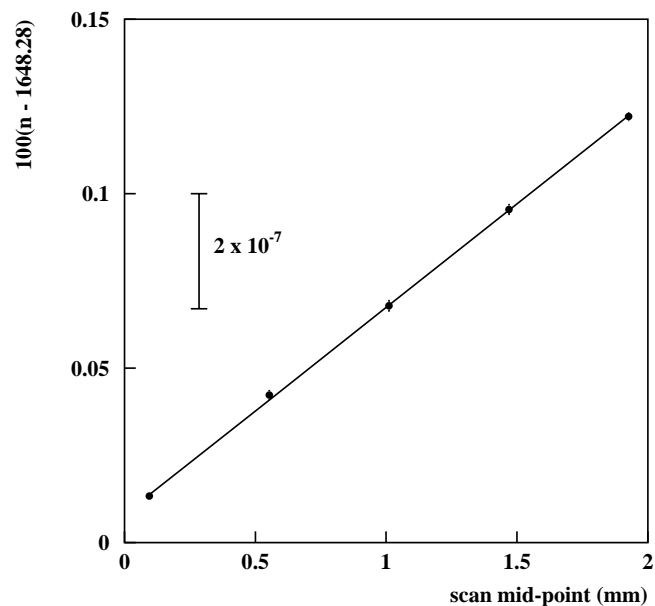


Fig. 9. Effect of the path curvature on n , the number of X-ray fringes per optical period. The solid line is the best fit of data to a straight line.

values $\alpha_z = (28.7 \pm 0.6) \mu\text{rad}$ and $\alpha_z = (27.8 \pm 0.3) \mu\text{rad}$ are derived from $R = 90$ mm and the data in Figures 8 and 9. These values can be compared with $\alpha_z = (29.6 \pm 0.7) \mu\text{rad}$, measured by means of X-ray diffractometry and given in [26]. The final d_{220} value was obtained by centering the analyser displacement on the path point whose tangent bisects α_z , thus ensuring that the displacement components measured by the X-rays and the laser interferometer coincide [27].

Other errors are caused by the way the guiding system is driven [20]. The crystal movement undergoes minute oscillations with periodicity $\Lambda \approx 0.11$ mm and amplitude $A \approx 10$ nm. In order to investigate the effect of these undulations, let us write the analyser position as

$$\mathbf{u}(s) = s\mathbf{e}_x + A \sin(2\pi s/\Lambda)\mathbf{e}_y, \quad (5)$$

where \mathbf{e}_y is orthogonal to \mathbf{e}_x and lies in the plane of the undulations. The phase of traveling X-ray fringes *versus* the result of the position measurement is

$$\Phi(s) = h \left[s + A\alpha_y \sin(2\pi s/\Lambda) \right], \quad (6)$$

where $\alpha_y = \mathbf{h} \cdot \mathbf{e}_y/h$ is the ‘‘horizontal’’ component of $\boldsymbol{\alpha}$. Owing to the small value of the undulation amplitude, and since $\alpha_y \approx 0.1$ mrad, the excess phase might appear to be lost in the hs term, and detection of the phase oscillations beyond present capabilities of X-ray and optical interferometry. However, the undulations have a detectable effect on the lattice spacing measurement. In fact,

$$d_{220} \approx \frac{1}{n} \left[\Delta s + 2A\alpha_y \sin(\pi \Delta s/\Lambda) \cos(2\pi \tilde{s}/\Lambda) \right], \quad (7)$$

where n is the number of traveling X-ray fringes in the scan Δs and \tilde{s} is the scan mid-point. The results of the d_{220} measurement may thus be expected to oscillate as much as the crystal path, but with an amplitude modulated by $\sin(\pi \Delta s/\Lambda)$. We varied Δs from $893\lambda/2$ (about 2.5Λ) to $1000\lambda/2$ (about 2.8Λ) and to $1048\lambda/2$ (about 3Λ). Actually, for each given Δs value, the scan mid-point was shifted in $40\lambda/2$ (about 0.1Λ) steps and the number of traveling X-ray fringe was measured in 18 adjacent (partially overlapping) fractions of the analyser path. Results are shown in Figure 10: the forward differences of the phase waveform generated by crystal motion produce oscillations, whose amplitude is maximum when $\Delta s = p\Lambda/2$ and zero when $\Delta s = p\Lambda$, with p integer, as expected. The final d_{220} value was obtained by counting the number of X-ray fringes per $1048\lambda/2$ displacement.

4.6 Crystal attitude

In order to keep Abbe’s error (the combined effect of analyser rotation and offset between the X-rays and the laser beam) to a minimum, adjacent parts of the optical interference pattern are integrated over the four parts of a quadrant detector and information about wavefront tilts are derived. Null pitch and yaw angles are thus measured to within 0.5 nrad, and the error signals are used to automatically keep the analyser parallel during its movement. In applying this technique to eliminate rotations, we observed an unexpected behaviour of the combined X-ray and optical interferometer, which we summarise in Figure 11. The pitch angle, which is nulled by the feedback of the optical error signal, is simultaneously and independently monitored by X-rays. The X-ray measuring principle is as simple as the optical one. Top and bottom parts

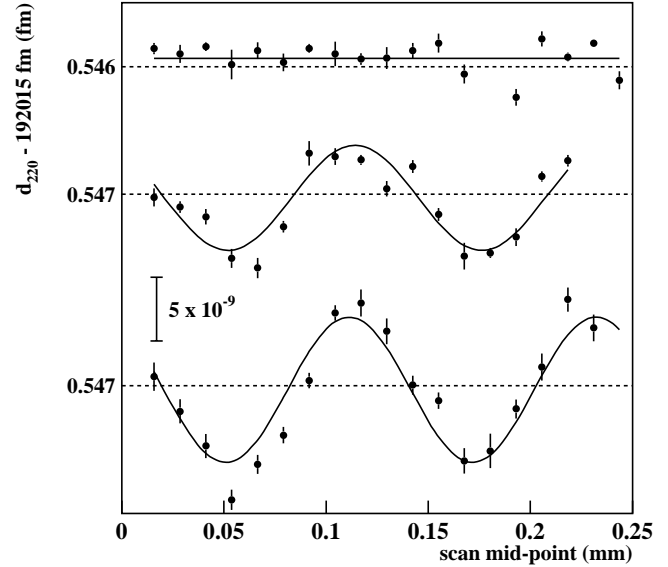


Fig. 10. Effect of the path undulation on the result of the d_{220} measurement. The curves refer to different displacements (from top to bottom: $1048\lambda/2$, $1000\lambda/2$, $893\lambda/2$) and have been shifted vertically with respect to each other. The effect of path curvature has been removed. The solid lines are the best fit of data to the predicted function.

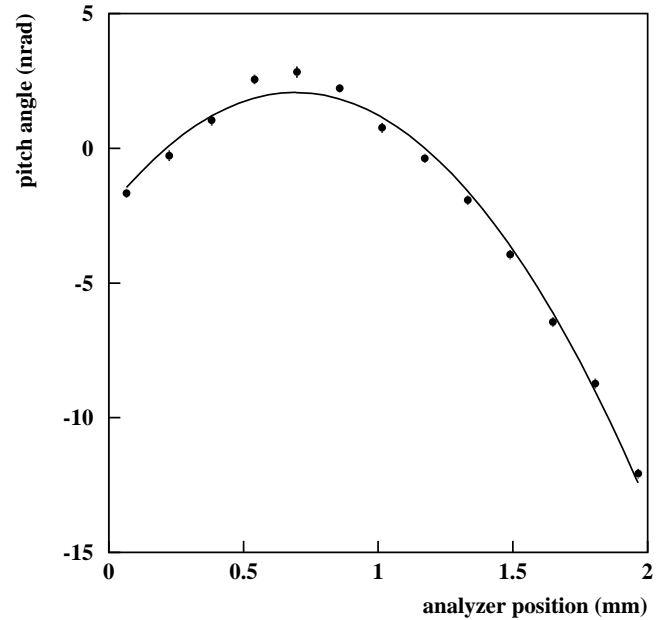


Fig. 11. X-ray measurement of the pitch angle. The solid lines is the best fit of data to a parabola.

of the X-ray interference pattern are integrated over two parts of a position-sensitive detector. The crystal movement is thus measured at two points spaced vertically by a few millimeters: any rotation reveals itself as a relative advance or delay of traveling X-ray fringes. As shown in Figure 11, X-rays reveal that, despite the action of the electronic pitch control, the crystal rotates. Two features are evident in Figure 11. First, the pitch angle drifts with

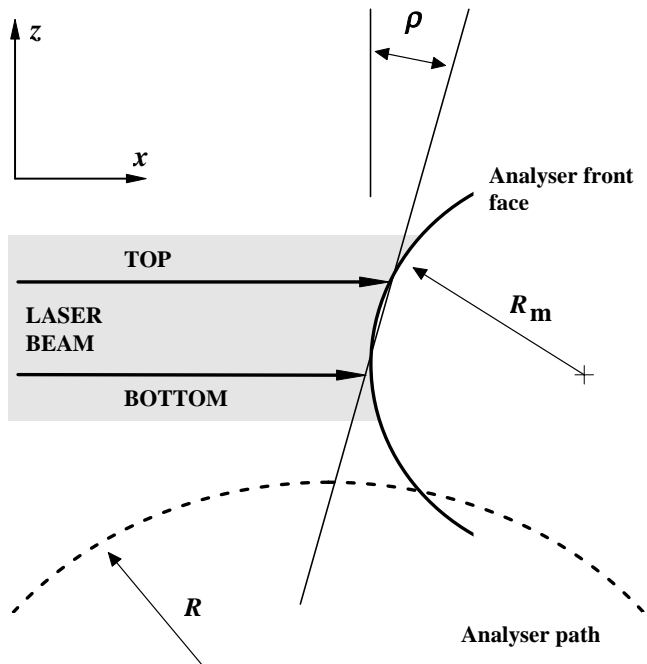


Fig. 12. Geometry of the pitch-angle measurement by the laser interferometer.

displacement. This phenomenon has been explained as due to imperfect alignment between the optical axes of the laser beam and of the interferometer (the normal to the analyser front face) [19]. Second, the millimetre displacement brought into evidence a quadratic term, which was unnoticed in our previous investigations.

We carried out many different experiments which ruled out the possibility of this phenomenon being due to non-uniform lattice strains or to aberrations of the laser beam wavefront. In our opinion, it is a measurement error of the angle-interferometer which is due to the combined effect of circular path and curvature of the front mirror. Since, owing to path circularity, the analyser moves vertically, the angle interferometer performs the derivative of its front surface, as shown in Figure 12. For the sake of simplicity, let us consider a two-dimensional mirror surface described by $x = z^2/(2R_m)$, where R_m is the curvature radius. In the absence of pitch rotations, the angle signal is $\rho = dx/dz = z/R_m$, where z is the vertical position of the analyser. Thus, since from (3) $z = s^2/(2R)$, the measurement error is

$$\rho = \frac{s^2}{2RR_m}. \quad (8)$$

This error is corrected for by rotating the analyser by a counter sign angle, detected by X-rays, and reported in Figure 11. The radius of curvature of the analyser front face estimated from the data in the figure is 600 m. In order to check the notion that this anomaly corresponds to a “spherical” mirror, the PTB measured the flatness of the analyser front face. Although, on average, the front face is very flat, it presents undulations having a “wavelength” of a few millimeters and an amplitude of about 10 nm (peak

to valley). Therefore, within the limits of the present data, the radius of curvature estimated from data in Figure 11 is consistent with the distortion found.

5 Outlooks

This article provides new accurate values of the (220) lattice-plane spacing of the MO*4 standard, supplements the analysis of its error budget and gathers evidence of important new advances in the measurements of macroscopic displacements with picometer-scale resolution. Our new set-up proved able to reduce systematic errors to a magnitude of $10^{-9}d_{220}$ and observations led us to confirm the d_{220} value we gave previously [11]. This value should be compared with that reported in [7] for the PTB standard WASO 4.2A. In order to check the consistency of these two absolutely measured lattice spacings, the PTB performed a comparison between the MO*4 and WASO 4.2A standards. The difference between the two absolute values [7, 11],

$$d_{220}^{\text{WASO4.2A}} - d_{220}^{\text{MO*4}} = (6 \pm 6) \times 10^{-8}d_{220}, \quad (9a)$$

can be compared with the expected difference of lattice spacings due to their different carbon and oxygen contamination [28],

$$d_{220}^{\text{WASO4.2A}} - d_{220}^{\text{MO*4}} = (7 \pm 3) \times 10^{-8}d_{220}, \quad (9b)$$

and with the comparison result [29],

$$d_{220}^{\text{WASO4.2A}} - d_{220}^{\text{MO*4}} = (10 \pm 1) \times 10^{-8}d_{220}. \quad (9c)$$

These data shows that the difference between the absolute (220) lattice-plane spacing values of WASO 4.2A and MO*4 standards can be explained by an actual lattice-plane spacing difference, probably due to their different contaminations.

We conclude that a 10^{-9} relative uncertainty is within the capabilities of scanning X-ray and optical interferometry, but continued step-by-step improvements will be needed. The relatively poor geometrical and crystallographic quality of the MO*4 crystal is a limit. The growing of still better silicon crystals, a task pursued by Wacker Chemitronic, is among the topics considered by the *ad hoc* Working Group on the Avogadro Constant established in 1995 by the “Comité Consultatif pour la Masse of the Bureau International des Poids et Mesures”. In the immediate future we need to improve etching of X-ray interferometers to make it geometrically comparable with grinding. The particular problem still remains that movement is not along a straight line and that the transverse components of the movement are not under control. In this connection, over the next years, we aim to develop a five-degrees-of-freedom positioning system capable of controlling actively the transverse movements to within 1 nm resolution.

We cordially thank our PTB colleagues P. Becker and U. Kuetgens for the loan of their WASO 4.2A interferometer, the front-face flatness measurement, and the lattice comparison.

References

1. E.R. Cohen, B.N. Taylor, *Rev. Mod. Phys.* **57**, 1121 (1987).
2. G.L. Greene *et al.*, *Phys. Rev. Lett.* **56**, 819 (1986).
3. P. Becker, G. Mana, *Metrologia* **31**, 203, (1994).
4. G. Mana, G. Zosi, *Riv. Nuovo Cimento* **18**, 1 (1995).
5. E. Krüger *et al.*, *Metrologia* **32**, 117 (1995).
6. R.D. Deslattes, A. Henins, *Phys. Rev. Lett.* **31**, 972 (1973).
7. P. Becker *et al.*, *Phys. Rev. Lett.* **46**, 1540 (1981).
8. P. Becker *et al.*, *Z. Phys. B* **48**, 17 (1982).
9. G. Basile *et al.*, *IEEE Trans. Instrum. Meas.* **38**, 210 (1989).
10. G. Basile *et al.*, *IEEE Trans. Instrum. Meas.* **40**, 98 (1991).
11. G. Basile *et al.*, *Phys. Rev. Lett.* **72**, 3133 (1994).
12. G. Basile *et al.*, *IEEE Trans. Instrum. Meas.* **44**, 526 (1995).
13. H. Fujimoto *et al.*, *J. Appl. Phys.* **34**, 5065 (1995).
14. A. Bergamin *et al.*, *IEEE Trans. Instrum. Meas.* **46**, 576 (1997).
15. A. Bergamin, G. Cavagnero, G. Mana, *Meas. Sci. Technol.* **2**, 725 (1991).
16. B. Edlen, *Metrologia* **2**, 71 (1986).
17. A. Bergamin *et al.*, *J. Appl. Phys.* **82**, 5396 (1997).
18. G. Mana, *Metrologia* **26**, 87 (1989).
19. A. Bergamin, G. Cavagnero, G. Mana, *Phys. Rev. A* **49**, 2167 (1994).
20. A. Bergamin *et al.*, *IEEE Trans. Instrum. Meas.* **46**, 196 (1997).
21. A. Bergamin *et al.*, *Eur. Phys. J. D* **5**, 433 (1999).
22. A. Accotto, E. Vittone, G. Zosi, *Z. Phys. B* **95**, 151 (1994).
23. E. Vittone, G. Zosi, *Metrologia* **31**, 211 (1994).
24. G. Mana, E. Vittone *Z. Phys. B* **102**, 189 (1997).
25. G. Mana, E. Vittone *Z. Phys. B* **102**, 197 (1997).
26. H. Siegert, P. Becker, in *Precision Measurements and Fundamental Constants II*, edited by B.N. Taylor and W.D. Phillips (Natl. Bur. Stand., Gaithersburg, 1984), p. 321.
27. G. Basile *et al.*, *IEEE Trans. Instrum. Meas.* **40**, 98 (1991).
28. G. Basile *et al.*, *IEEE Trans. Instrum. Meas.* **44**, 538 (1995).
29. J. Martin *et al.*, *Metrologia* **35**, 811 (1999).